Electronic supplementary materials

Two 6/10-connected $Cu_{12}S_6$ cluster-based organic frameworks: crystal structure and proton conduction

Jia-Ming Li[a*], Tian-Yang Xu[a,b], Ya-Li Zhao[a], Xing-Liang Hu[b], Kun-Huan He[a*]

[a] Qinzhou Key Laboratory for Development and Application of High Performance Functional Materials, College of Petroleum and Chemical Engineering, Beibu Gulf University, Qinzhou 535011 People's Republic of China

[b] School of Chemistry and Pharmacy, Guangxi Normal University, Key Laboratory for the Chemistry and Molecular Engineering of Medicinal Resources (Ministry of Education), Guilin 541004 People's Republic of China

Corresponding Author

*Email: jmli@bbguu.edu.cn (Jia-Ming Li)

*Email: hkh821227@163.com (Kun-Huan He)

1. Experimental section

1.1. Materials and physical measurements

All chemical reagents were purchased from Jinan Henghua Sci. & Tec. Co. Ltd. without further purification. Powder X-ray diffraction (PXRD) data were collected on a Bruker D8 ADVANCE X-ray diffractometer with Cu-Kα radiation (λ = 1.5418 Å) at 40 kV, 40 mA with a scanning rate of 6°/min and a step size of 0.02°. The simulation of the PXRD spectra was carried out by the single-crystal data and diffraction-crystal module of the Mercury 2.0 (Hg) program available free of charge via the Internet at http://www.iucr.org. The purity and homogeneity of the bulk products were determined by comparing the simulated and experimental X-ray powder diffraction patterns (Figure S1). Elemental analyses (EA) for C, H, N and S were performed on an EA1110 CHNSO CE elemental analyzer (Figure S2). FT-IR spectra were recorded in the range of 4000–450 cm^{-1} on a PerkinElmer Frontier spectrometer (Figure S3). Thermogravimetric analyses (TG) were performed under nitrogen with a heating rate of $10^0C\ min^{-1}$ using a PerkinElmer Thermogravimetric Analyzer TGA4000. The Alternating Current (AC) impedance analysis was carried out on a Zennium X electrochemical workstation by the three electrode method. Transmission Electron Microscope (TEM) measurements were obtained with Talos F200 (Figure S4). Hirshfeld surface analyses were calculated by using the CrystalExplorer 17.[1] Point symbol and topological analyses were conducted by using the TOPOS 4.0 program package.[2]

1.2. X-ray crystallography

Suitable single crystals of MOFs **1** and **2** were selected and glued to thin glass fibers. Intensities data for crystal structure analysis of compounds **1** and **2** were collected at 298 K with Mo-Kα radiation (λ = 0.71073 Å) on a Rigaku XtaLAB Mini (ROW) diffractometer equipped with CCD. The instrument was controlled with CrysAlisPro software package,[3] which was used for collecting the diffraction images, absorption correction, and data reduction. Using Olex2,[4] the structure was solved with the ShelXT structure solution program using Intrinsic Phasing[5] and refined with the ShelXL refinement package using Least Squares minimization[6]. Carbon-bound H

atoms were placed in calculated positions ($d_{C–H}$ = 0.97 Å) and were included in the refinement in the riding model approximation, with U_{iso}(H) set to 1.2U_{eq}(C). The H atoms of coordinated and solvent water in **1** and **2** were also positioned geometrically and refined as riding atoms, with $d_{O–H}$ = 0.82-0.90 Å and U_{iso}(H) = 1.5U_{eq}(O). There is some displacement disorder C/O/S-atoms from the 2-mercaptoethanesulfonic acid and 3-mercaptopropanesulfonic acid in **1** and **2**. Therefore, the PART 1 and PART 2 introductions implemented in Olex2 were used to divide these atoms into two disordered groups. The disordered atoms were refined with an occupancy ratio of 0.63:0.37 for **1**, and 0.90:0.10 for **2**. A maximal residual electron density peak 3.35 e $Å^{-3}$ is close to 1.1 Å from Cu4 in **1**. So, the copper atom Cu4 in **1** has been split into two parts and refined with an occupancy ratio of 0.82:0.18. Subsequently, the appropriate restraint or constraint instructions SADI, EADP and DFIX from ShelXL were applied to constrain the displacement parameters of those disordered atoms. The structures were examined using the Addsym subroutine of PLATON[7] to ensure that no additional symmetry could be applied to the models. The total potential solvent accessible void volume (SOLV-Map Value) about 38 $Å^3$ is found in **1** [about 1% (38 $Å^3$) of the unit cell volume (3962.8 $Å^3$)] using the PLATON program. Pertinent crystallographic data collection and refinement parameters are collated in Table S1. Selected bond lengths and angles, and hydrogen-bond geometry are organized in Tables S2-S7. CCDC 2024526 (**1**) and 2024527 (**2**) contain the supplementary crystallographic data for this paper. These data can be obtained free of charge from The Cambridge Crystallographic Data Centre via http://www.ccdc.cam.ac.uk/data request/cif.

1.3. Synthesis of $[Cu_{12}(MES)_6(H_2O)_3]_n$ (1)

$Cu(NO_3)_2·3H_2O$ (0.242 g, 1 mmol), sodium 2-mercaptoethanesulfonate (0.083 g, 0.5 mmol), 1,3-bis (4-pyridyl) propane (0.100 g, 0.5 mmol), H_2O (15 ml) were sealed in a 25ml Teflon-lined reactor at 120℃ for 3 days. After gradually cooling to room temperature at a rate of 6 °C h^{-1}, yellow block-shaped of **1** was obtained (Yield: 60%). Elemental analysis (EA) calc. (%) for $C_{12}H_{30}Cu_{12}O_{21}S_{12}$ (**1**), M_r = 1657.56: C, 8.69; H, 1.81; S, 23.17. Found: C, 8.66; H, 1.84; S, 23.21.

1.4. Synthesis of $\{[Cu_{12}(MPS)_6(H_2O)_4]\cdot 6H_2O\}_n$ (2)

The synthesis of **2** is similar to that for **1** except for sodium 2-mercaptoethanesulfonate (0.083 g, 0.5 mmol) substituted for sodium 2-mercaptopropanesulfonate (0.088 g, 0.5 mmol). Similarly, yellow block-shaped of **2** was obtained (Yield: 50%). Elemental analysis *calc.* for $C_{18}H_{56}Cu_{12}O_{28}S_{12}$ (**2**), M_r = 1867.82: C, 11.56; H, 3.00; S, 20.56. Found: C, 11.54; H, 3.02; S, 20.57.

1.5. Reaction mechanism of synthesis for 1 and 2

Interestingly, the synthesis of **1** and **2** rely on subtle control over various hydrothermal parameters, particularly the starting materials. In the process of synthesis of **1** and **2**, we had attempted to directly use the univalent or divalent copper salts to react with the 2-mercaptoethanesulfonate or sodium 2-mercaptoethanesulfonate ligand. No matter how to change and combine to be considered various conditions, unfortunately, we can not get the target product. In comparison, we had also tried to apply the univalent copper salts to react with the combination of 2-mercaptoethanesulfonate or sodium 2-mercaptoethanesulfonate and 1,3-bis (4-pyridyl) propane ligands under various conditions. The same results are obtained as above. In summary, the optimum solution is to combine the three substances Cu(II) salt, sodium 2-mercaptoethanesulfonate and 1,3-bis (4-pyridyl) propane at the same time. We infer the first step probably is a redox reaction that Cu^{2+} cation acts as an oxidant and 1,3-bis (4-pyridyl) propane as a reductant in this synthesis. This ratiocination is consistent with the obtained reaction products, which contain both the title Cu(I)-based organic framework and diaqua-bis(pyridine-4-carboxylate-N)-copper(II) monohydrate and were confirmed by single-crystal X-ray diffraction. Therefore, taking the synthesis of **1** as its sample, the recommended two step successive reaction equations are as follow.

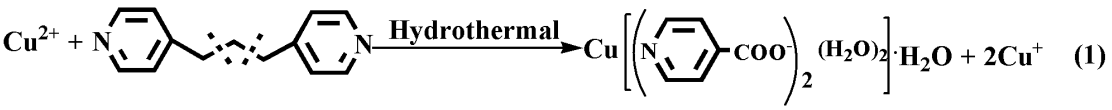

$$12Cu^{+} + 6^{-}O_3SCH_2CH_2S^{-} \xrightarrow{\text{Hydrothermal}} [Cu_{12}(O_3SCH_2CH_2S)_6(H_2O)_3]_n \quad (2)$$

1.6. Proton conductivity measurement

The Alternating Current (AC) impedance spectrums of composite membrane

stemmed from MOFs **1** and **2** were measured on a Zennium X electrochemical workstation with a three-electrode system. The working electrode was the MOFs/Nafion composite membrane modified glass carbon electrode (GCE). Platinum plate is the reference electrode and the counter electrode. The electrolyte solution is 0.1M potassium aqueous solution. The AC impedance data were obtained at an applied potential of 500 mV and frequency ranging from 1 to 1×10^6 Hz, and cycle back and forth twice.

The composite membrane was prepared according to the document[8] and as following procedure: first, the bare GCE was polished carefully with 0.3 μm alumina slurry and cleaned successively with water. 1.0 mg MOFs sample was ultrasonically dispersed into 500 μL water to form homogeneous MOFs solution. 100 μL pure Nafion was add to 400 μL water to form Nafion diluent. Then, 5 μL MOFs solution and 5 μL Nafion diluent were mixed under ultrasonic condition. The mixture was placed onto the GCE surface, and dry at room temperature, then put in oven, drying under the temperature of 60 ^{o}C for 0.5 h.

2. Thermal stabilities

The thermogravimetric (TG) analyses the thermal decomposition behaviors of MOFs **1** and **2** have been performed in a nitrogen atmosphere at a heating rate of 10 °C min^{-1} between 25 and 1000 °C to confirm their thermal stability (Figure S23). For MOF **1**, a weight loss of 3.22% was observed in the region 120–290 °C, which is attributed to the release of the three coordinated water molecules (calcd. 3.26%). For MOF **2**, a continuously sharp weight loss of 10.02% was observed in the region 90–150 °C, which is attributed to the release of the six free and four coordinated H_2O molecule (calcd. 9.64%). It can be observed from TG curves that the two MOFs could maintain their structural framework up to 300 °C for **1** and 220 °C for **2**. Above these temperatures, both MOFs display a sharply thermogravimetric process corresponding to the thermal decomposition of organic components. Finally, a plateau region from 900 to 1000 °C for **1** (from 940 to 1000 °C for **2**) can be found in the TG curves. The final black residues were about 51.16% (calcd. 51.76%) and 45.84 (calcd. 45.94%) of the initial total weight

for **1** and **2**, respectively, which may be Cu_2O.

References

1 M. J. Turner, J. J. McKinnon, S. K. Wolff, D. J. Grimwood, P. R. Spackman, D. Jayatilaka, M. A. Spackman, *Crystal-Explorer17*, University of Western Australia, Perth, Australia, 2017.

2 V. A. Blatov, *IUCr CompComm Newsletter*, 2006, **7**, 4-38.

3 Rigaku Oxford Diffraction. CrysAlisPro Software System, Version 1.171.40.25a, Rigaku Corporation: Oxford, UK, 2018.

4 O. V. Dolomanov, L. J. Bourhis, R. J. Gildea, J. A. K. Howard, H. Puschmann, *J. Appl. Crystallogr*., 2009, **42**, 339–341.

5 G. M. Sheldrick, *Acta. Crystallogr. Sect. A*, 2015, **71**, 3-8.

6 G. M. Sheldrick, *Acta. Crystallogr. Sect. C*, 2015, **71**, 3–8.

7 A. L. Spek, *Acta. Crystallogr. Sect. D*, 2009, **65**, 148–155.

8 R. Y. Li, H. T. Liu, C. C. Zhou, Z. T. Chu, J. Lu, S. N. Wang, J. Jin, W. F. Yan, *Inorg. Chem. Front.*, 2020, **7**, 1880-1891.

Table S1 Crystal data and structure refinement for 1-2[a]

MOF	**1**	**2**
Empirical formula	$C_{12}H_{30}Cu_{12}O_{21}S_{12}$	$C_{18}H_{56}Cu_{12}O_{28}S_{12}$
Formula weight	1657.56	1867.82
Temperature/K	298.15	298.15
Crystal system	monoclinic	triclinic
Space group	$P2_1/c$	P-1
a/Å	11.8921(4)	12.4249(7)
b/Å	17.7132(6)	12.5351(9)
c/Å	18.9516(7)	19.7599(9)
α/°	90	72.310(5)
β/°	96.951(3)	82.128(4)
γ/°	90	60.367(7)
Volume/Å^3	3962.8(2)	2548.2(3)
Z	4	2
ρ_{calc}/g cm^{-3}	2.778	2.434
μ/mm^{-1}	7.004	5.470
F(000)	3240.0	1856.0
Crystal size/mm^3	0.25 × 0.2 × 0.15	0.25 × 0.2 × 0.15
Radiation	Mo Kα (λ = 0.71073)	Mo Kα (λ = 0.71073)
2Θ range for data collection/°	4.904 to 50.194	5.03 to 50.198
Index ranges	$-14 \le h \le 14$, $-21 \le k \le 20$, $-22 \le l \le 22$	$-14 \le h \le 14$, $-14 \le k \le 14$, $-23 \le l \le 23$
Reflections collected	16906	14516
Independent reflections	7036 [R_{int} = 0.0249, R_{sigma} = 0.0296]	9038 [R_{int} = 0.0188, R_{sigma} = 0.0283]
Data/restraints/parameters	7036/11/554	9038/18/665
Goodness-of-fit on F^2	1.047	1.022
Final R indexes [I>=2σ (I)]	R_1 = 0.0317, wR_2 = 0.0746	R_1 = 0.0337, wR_2 = 0.0841
Final R indexes [all data]	R_1 = 0.0421, wR_2 = 0.0787	R_1 = 0.0420, wR_2 = 0.0884
Largest diff. peak/hole / e Å^{-3}	0.844/-1.387	1.721/-1.418

[a] $R_1 = \Sigma||F_o| - |F_c|| / \Sigma|F_o|$, w$R_2 = [\Sigma w(F_o^2 - F_c^2)^2/\Sigma w(F_o^2)^2]^{1/2}$

Table S2. Selected bond lengths (Å) for 1

Bond	Length	Bond	Length	Bond	Length
Cu12-Cu7^{i}	2.8304(8)	Cu7-O9	2.159(3)	Cu1-O12^{x}	2.247(3)
Cu12-Cu1^{ii}	2.8781(9)	Cu6-Cu5^{xi}	2.8723(9)	Cu1-O1	2.211(4)
Cu12-Cu11^{iii}	2.9545(9)	Cu6-S4^{xi}	2.2510(12)	Cu5-Cu9^{xvi}	2.7887(9)
Cu12-Cu^{iv}	2.8429(12)	Cu6-S2^{viii}	2.2898(12)	Cu5-Cu4	2.7965(12)
Cu12-S11^{iii}	2.2348(12)	Cu6-O20^{xiii}	2.273(3)	Cu5-S2^{xvii}	2.2508(12)
Cu12-S4^{iv}	2.2524(12)	Cu6-O10	2.198(3)	Cu5-S5	2.3205(13)
Cu12-O18	2.120(3)	Cu1-Cu8^{xiv}	2.7681(9)	Cu5-O19^{xii}	2.280(4)
Cu3-Cu2^{v}	2.9258(9)	Cu1-S11^{xv}	2.2947(12)	Cu5-O8	2.123(4)
Cu3-Cu5^{vi}	2.8716(9)	Cu1-S9^{xiv}	2.2536(12)	Cu11-Cu9^{vii}	2.9162(9)
Cu3-Cu9^{vii}	2.8324(9)	Cu7-O11	2.180(4)	Cu11-S11	2.2165(12)
Cu3-Cu10^{vii}	2.9661(9)	Cu8-O13	2.140(4)	Cu11-S5^{vi}	2.2568(13)
Cu3-S2^{v}	2.2404(12)	Cu9-S5^{xviii}	2.2103(13)	Cu11-O16	2.023(4)
Cu3-S8^{vii}	2.2499(13)	Cu9-S8	2.2090(13)	Cu8-Cu9	2.9425(10)
Cu3-O5	2.029(6)	Cu9-O14	2.075(4)	Cu8-Cu10	2.9339(9)
Cu3-O5A	2.091(11)	Cu10-S9	2.2202(13)	Cu8-S11^{xii}	2.2630(12)
Cu2-Cu7^{viii}	2.9581(9)	Cu10-S8	2.1949(13)	Cu8-S8	2.3118(13)
Cu2-Cu6^{viii}	2.9687(9)	Cu10-O15	2.013(5)	Cu8-O2^{xvii}	2.246(4)
Cu2-Cu10^{ix}	2.8887(9)	Cu4-S4	2.2166(14)	C3-S3	1.775(9)
Cu2-S2	2.2169(12)	Cu4-S5	2.2039(14)	S3-O4	1.464(10)
Cu2-S9^{ix}	2.2589(13)	Cu4-O7	2.002(4)	S3-O5	1.468(7)
Cu2-O4	2.107(12)	S11-C11	1.842(5)	S3-O6	1.446(7)
Cu2-O4A	1.96(2)	S4-C4	1.840(8)	S8-C8	1.837(5)
Cu7-Cu6	2.8790(9)	S4-C4A	1.857(14)	S5-C5	1.834(5)
Cu7-Cu1^{x}	2.8294(9)	S2-C2	1.844(5)	S10-O18	1.456(3)
Cu7-S4^{xi}	2.2828(13)	S9-C9	1.833(5)	S10-O16	1.464(4)
Cu7-S9^{xii}	2.2751(13)	S6-O10	1.478(4)	S10-O17	1.425(5)
S7-C7	1.777(5)	S6-O9	1.461(4)	S10-C10	1.793(6)
S12-O20	1.457(4)	S6-O8	1.453(4)	S1-O2	1.473(4)
S12-O21	1.457(4)	S6-C6	1.777(5)	S1-O3	1.460(4)
S12-O19	1.470(4)	S7-O12	1.472(4)	S1-O1	1.466(4)
S7-O13	1.455(4)	S12-C12	1.779(5)	S1-C1	1.779(5)

Symmetry codes: (i) −*x*+1, −*y*+1, −*z*+2; (ii) *x*, *y*, *z*+1; (iii) −*x*+1, −*y*, −*z*+2; (iv) *x*+1, −*y*+1/2, *z*+1/2; (v) −*x*, −*y*, −*z*+1; (vi) −*x*, *y*−1/2, −*z*+3/2; (vii) −*x*+1, *y*−1/2, −*z*+3/2; (viii) −*x*, −*y*+1, −*z*+1; (ix) *x*−1, −*y*+1/2, *z*−1/2; (x) −*x*+1, −*y*+1, −*z*+1; (xi) −*x*, *y*+1/2, −*z*+3/2; (xii) −*x*+1, *y*+1/2, −*z*+3/2; (xiii) *x*−1, *y*+1, *z*; (xiv) *x*, −*y*+1/2, *z*−1/2; (xv) −*x*+1, −*y*, −*z*+1; (xvi) *x*−1, *y*, *z*; (xvii) *x*, −*y*+1/2, *z*+1/2; (xviii) *x*+1, *y*, *z*.

Table S3. Selected bond angles (˚) for 1

Bond angle	Degree	Bond angle	Degree	Bond angle	Degree
Cu7^{i}-Cu12-Cu1^{ii}	59.42(2)	O2^{xviii}-Cu8-S8	112.86(10)	O5-Cu3-Cu5^{vii}	128.71(18)
Cu7^{i}-Cu12-Cu11^{iii}	128.41(3)	O13-Cu8-Cu1^{xviii}	161.33(10)	S8-Cu10-S9	131.05(5)
Cu7^{i}-Cu12-Cu4^{iv}	94.52(3)	O13-Cu8-Cu9	76.69(12)	S9-Cu10-Cu2^{iv}	50.43(3)
Cu1^{ii}-Cu12-Cu11^{iii}	92.82(2)	O13-Cu8-Cu10	133.15(10)	S9-Cu10-Cu8	100.14(4)
Cu4^{iv}-Cu12-Cu1^{ii}	128.56(3)	O13-Cu8-S11^{xii}	111.46(10)	S8-Cu10-Cu3^{xii}	48.94(3)
Cu4^{iv}-Cu12-Cu11^{iii}	68.59(2)	O13-Cu8-S8	91.31(11)	S8-Cu10-Cu2^{iv}	105.16(4)
S11^{iii}-Cu12-Cu7^{i}	108.58(4)	O13-Cu8-O2^{xviii}	91.43(15)	S8-Cu10-Cu8	51.14(3)
S11^{iii}-Cu12-Cu1^{ii}	51.48(3)	Cu3^{xii}-Cu9-Cu11^{xii}	135.57(3)	S8^{vi}-Cu3-Cu2^{v}	102.54(4)
S11^{3}Cu12Cu11^{3}	48.15(3)	Cu3^{xii}-Cu9-Cu8	94.34(3)	S8^{v}-Cu3-Cu5^{vii}	104.72(4)
S11^{iii}-Cu12-Cu4^{iv}	113.78(4)	Cu5^{xix}-Cu9-Cu3^{xii}	61.44(2)	S8^{vi}-Cu3-Cu9^{vi}	49.93(3)
S11^{iii}-Cu12-S4^{iv}	143.83(5)	Cu5^{xix}-Cu9-Cu11^{xii}	96.42(3)	S8^{vi}-Cu3-Cu10^{vi}	47.35(3)
S4^{iv}-Cu12-Cu7^{i}	51.87(3)	Cu5^{xix}-Cu9-Cu8	122.95(3)	O5-Cu3-Cu2^{v}	130.50(18)
S4^{iv}-Cu12-Cu1^{ii}	108.99(4)	Cu11^{xii}-Cu9-Cu8	64.50(2)	O14-Cu9-S8	106.54(13)
S4^{iv}-Cu12-Cu11^{iii}	115.36(4)	S5^{xix}-Cu9-Cu3^{xii}	114.11(4)	Cu2^{iv}-Cu10-Cu3^{xii}	59.94(2)
S4^{iv}-Cu12-Cu4^{iv}	49.94(4)	S5^{xix}-Cu9-Cu5^{xix}	53.82(3)	Cu2^{iv}-Cu10-Cu8	120.02(3)
O18-Cu12-Cu7^{i}	127.32(9)	S5^{xix}-Cu9-Cu11^{xii}	49.94(3)	Cu8-Cu10-Cu3^{xii}	91.77(3)
O18-Cu12-Cu1^{ii}	125.33(11)	S5^{xix}-Cu9-Cu8	109.79(4)	S9-Cu10-Cu3^{xii}	105.20(4)
O18-Cu12-Cu11^{iii}	104.27(9)	S8-Cu9-Cu3^{xii}	51.20(3)	S2^{v}-Cu3-Cu2^{v}	48.63(3)
O18-Cu12-Cu4^{iv}	105.92(11)	S8-Cu9-Cu5^{xix}	108.63(4)	S2^{v}-Cu3-Cu5^{vii}	50.41(3)
O18-Cu12-S11^{iii}	106.38(11)	S8-Cu9-Cu11^{xii}	114.56(4)	S2^{v}-Cu3-Cu9^{vi}	105.80(4)
O18-Cu12-S4^{iv}	109.28(11)	S8-Cu9-Cu8	50.93(3)	S2^{v}-Cu3-Cu10^{vi}	104.86(4)
Cu2^{v}-Cu3-Cu10^{vi}	58.72(2)	S8-Cu9-S5^{xix}	145.68(5)	S2^{v}-Cu3-S8^{vi}	135.16(5)
Cu5^{vii}-Cu3-Cu2^{v}	87.29(2)	O14-Cu9-Cu3^{xii}	111.51(13)	O14-Cu9-Cu8	119.10(11)
Cu5^{vii}-Cu3-Cu10^{vi}	116.27(3)	O14-Cu9-Cu5^{xix}	117.84(11)	O14-Cu9-S5^{ix}	107.77(13)
Cu9^{vi}-Cu3-Cu2^{v}	115.26(3)	O14-Cu9-Cu11^{xii}	112.91(13)	Cu9^{vi}-Cu3-Cu5^{vii}	58.53(2)
O5-Cu3-Cu5^{vii}	128.71(18)	S8-Cu10-S9	131.05(5)	Cu9^{vi}-Cu3-Cu10^{vi}	87.60(2)
O5-Cu3-Cu9^{vi}	112.85(18)	O15-Cu10-Cu3^{xii}	115.77(19)	O5-Cu3-S2^{v}	125.6(2)
O5-Cu3-Cu10^{vi}	113.40(18)	O15-Cu10-Cu2^{iv}	109.8(2)	O15-Cu10-Cu8	130.1(2)
O5-Cu3-S8^{vi}	99.3(2)	O15-Cu10-S9	110.31(16)	Cu3^{v}-Cu2-Cu7^{viii}	115.96(3)
O15-Cu10-S8	118.36(16)	Cu3^{v}-Cu2-Cu6^{viii}	91.21(2)	Cu7^{viii}-Cu2-Cu6^{viii}	58.12(2)
S4-Cu4-Cu12^{ix}	51.05(4)	Cu10^{ix}-Cu2-Cu3^{v}	61.34(2)	Cu5-Cu4-Cu12^{ix}	108.70(3)
Cu10^{ix}-Cu2-Cu6^{viii}	124.62(3)	S5-Cu4-Cu5	53.73(4)	S2-Cu2-Cu3^{v}	49.32(3)
S5-Cu4-S4	128.04(6)	S2-Cu2-Cu7^{viii}	102.70(4)	O7-Cu4-Cu12^{ix}	117.72(16)

Symmetry codes: (i) −*x*+1, −*y*+1, −*z*+2; (ii) *x*, *y*, *z*+1; (iii) −*x*+1, −*y*, −*z*+2; (iv) *x*+1, −*y*+1/2, *z*+1/2; (v) −*x*, −*y*, −*z*+1; (vi) −*x*, *y*−1/2, −*z*+3/2; (vii) −*x*+1, *y*−1/2, −*z*+3/2; (viii) −*x*, −*y*+1, −*z*+1; (ix) *x*−1, −*y*+1/2, *z*−1/2; (x) −*x*+1, −*y*+1, −*z*+1; (xi) −*x*, *y*+1/2, −*z*+3/2; (xii) −*x*+1, *y*+1/2, −*z*+3/2; (xiii) *x*−1, *y*+1, *z*; (xiv) *x*, −*y*+1/2, *z*−1/2; (xv) −*x*+1, −*y*, −*z*+1; (xvi) *x*−1, *y*, *z*; (xvii) *x*, −*y*+1/2, *z*+1/2; (xviii) *x*+1, *y*, *z*; (xix) *x*, *y*, *z*−1; (xx) *x*+1, *y*−1, *z*.

Table S4 Hydrogen-bond geometry (Å, º) for 1

D-H···A	D-H	H···A	D···A	D-H···A
O7-H7B···O17^{ix}	0.94	2.04	2.822 (7)	140
O7-H7A···O21^{ix}	0.94	2.03	2.849(7)	145
O15-H15B···O3^{xii}	0.91	1.90	2.805 (7)	169
O15-H15A···O3^{xvii}	0.90	2.40	3.118 (8)	136
O14-H14A···O10^{xviii}	0.87	2.01	2.857 (5)	165
C6-H6A···O4^{viii}	0.97	2.37	3.279 (13)	155
C6-H6B···O19^{xii}	0.97	2.43	3.233 (6)	140
C7-H7C···O18^{i}	0.97	2.51	3.418 (6)	156
C7-H7D···O15^{i}	0.97	2.65	3.445 (7)	139
C12-H12A···O17	0.97	2.44	3.314 (7)	149
C12-H12B···O2^{xv}	0.97	2.41	3.359 (6)	166
C5-H5A···O21^{ix}	0.97	2.50	3.306 (6)	140
C5-H5B···O14^{xvi}	0.97	2.73	3.407 (7)	128
C8-H8A···O3^{xii}	0.97	2.42	3.250 (6)	143
C8-H8B···O14	0.97	2.74	3.412 (7)	127
C11-H11B···O12^{xix}	0.97	2.65	3.387 (6)	133
C1-H1B···O20^{xv}	0.97	2.28	3.242 (6)	171
C10H10A···O13^{vii}	0.97	2.44	3.406 (7)	172
C10-H10B···O1^{xvii}	0.97	2.56	3.320 (7)	136
C3-H3A···O8^{vi}	0.97	2.45	3.395 (15)	164
C3-H3B···O20^{xii}	0.97	2.78	3.473 (9)	129
C9-H9A···O9^{vii}	0.97	2.67	3.322 (7)	125
C4-H4A···O11^{vi}	0.97	2.63	3.315 (14)	128

Symmetry codes: (i) $-x+1, -y+1, -z+2$; (vi) $-x, y-1/2, -z+3/2$; (vii) $-x+1, y-1/2, -z+3/2$; (viii) $-x, -y+1, -z+1$; (ix) $x-1, -y+1/2, z-1/2$; (xii) $-x+1, y+1/2, -z+3/2$; (xv) $-x+1, -y, -z+1$; (xvi) $x-1, y, z$; (xvii) $x, -y+1/2, z+1/2$; (xviii) $x+1, y, z$; (xix) $x, y-1, z$

Table S5. Selected bond lengths (Å) for 2

Bond	Length	Bond	Length	Bond	Length
Cu10-Cu11^{i}	2.6968(6)	Cu1-S1	2.2577(9)	Cu8-S1^{viii}	2.2789(9)
Cu10-Cu8^{ii}	2.7851(6)	Cu1-S7^{xi}	2.2549(10)	Cu8-O21	2.093(2)
Cu10-Cu2^{iii}	2.6660(6)	Cu1-O12^{vi}	2.262(2)	Cu8-O16	2.260(2)
Cu10-S5^{ii}	2.2223(8)	Cu1-O19	2.065(3)	Cu2-Cu12^{ix}	2.6838(6)
Cu10-S7	2.2041(8)	S9-C13	1.818(3)	Cu2-S1	2.2111(9)
Cu10-O13	2.121(2)	S11C16	1.831(3)	Cu2-S7^{iii}	2.2371(9)
Cu3-Cu7^{iii}	2.7396(6)	S5-C7	1.835(3)	Cu2-O18^{viii}	2.241(3)
Cu3-Cu4	2.6376(6)	S3-C4	1.831(3)	Cu12-S5^{vii}	2.2456(9)
Cu3-Cu9	2.6619(6)	S6-O7	1.462(2)	Cu12-S7^{x}	2.2552(9)
Cu3-S11	2.2458(8)	S6-O8	1.454(2)	Cu12-O17^{vii}	2.285(13)
Cu3-S3^{vi}	2.1966(8)	S6-O9	1.450(3)	Cu12-O10	2.114(2)
Cu3-O2	2.113(2)	S6-C9	1.757(3)	Cu5-S9^{iii}	2.2785(9)
Cu7-Cu9	2.7177(6)	S1-C1	1.821(4)	Cu5-S3^{v}	2.2268(9)
Cu7-Cu6	2.6703(6)	S7-C10	1.838(3)	Cu5-O4	2.213(2)
Cu7-S9	2.2023(8)	S10-O13	1.465(2)	Cu5-O20	2.074(3)
Cu7-S3^{v}	2.2617(9)	S10-O15	1.451(3)	Cu8-Cu1^{viii}	3.0276(7)
Cu7-O7	2.086(2)	S10-O14	1.438(3)	Cu8-S5	2.2432(9)
Cu4-S9^{iii}	2.2525(9)	S10-C15	1.753(3)	Cu11-S5^{vii}	2.2758(8)
Cu4-S11	2.2855(8)	S4-O5	1.456(2)	Cu11-S1^{vi}	2.2429(9)
Cu4-O5	2.132(2)	S4-O4	1.455(2)	Cu11-O11	2.184(2)
Cu4-O1	2.150(3)	S4-O6	1.456(2)	Cu11-O15^{iv}	2.213(3)
Cu9-Cu5^{iii}	2.7691(6)	S4-C6	1.761(3)	Cu8-Cu2^{viii}	2.6679(6)
Cu9-S9	2.2339(9)	S8-O11	1.459(2)	S12-O18	1.475(4)
Cu9-S11	2.2209(9)	S8-O12	1.458(2)	S12-O17	1.467(6)
Cu9-O22	2.055(2)	S8-O10	1.459(2)	S12-O16	1.454(2)
Cu6-S11	2.2509(9)	S8-C12	1.765(3)	S12-C18	1.752(9)
Cu6-S3^{v}	2.2799(9)	S2-O2	1.466(3)	S2-O1	1.433(3)
Cu6-O8	2.205(2)	S2-O3	1.422(3)	S2-C3	1.740(5)
Cu6-O6	2.112(2)	Cu11-Cu2^{vi}	2.8777(6)	Cu11-Cu12	3.0323(7)

Symmetry codes: (i) $x, y-1, z$; (ii) $-x+1, -y+1, -z$; (iii) $-x+1, -y+1, -z+1$; (iv) $x, y+1, z$; (v) $-x+1, -y, -z+1$; (vi) $-x+1, -y+2, -z+1$; (vii) $-x+1, -y+2, -z$; (viii) $-x, -y+1, -z+1$; (ix) $x-1, y-1, z+1$; (x) $-x+2, -y+2, -z$; (xi) $x-1, y, z+1$; (xii) $x+1, y+1, z-1$; (xiii) $x+1, y, z-1$.

Table S6. Selected bond angles (°) for 2

Bond angle	Degree	Bond angle	Degree	Bond angle	Degree
Cu11^{i}-Cu10-Cu8^{ii}	99.414(19)	S3^{v}-Cu5-Cu9^{iii}	97.44(3)	C13-S9-Cu9	112.66(12)
Cu2^{iii}-Cu10-Cu11^{i}	64.902(16)	S3^{v}-Cu5-S9^{iii}	125.23(3)	C13-S9-Cu5^{iii}	107.72(13)
Cu2^{iii}-Cu10-Cu8^{ii}	118.04(2)	O4-Cu5-Cu9^{iii}	149.88(7)	Cu3-S11-Cu4	71.19(3)
S5^{ii}-Cu10-Cu11^{i}	54.08(2)	O4-Cu5-S9^{iii}	102.27(7)	Cu3-S11-Cu6	133.26(4)
S5^{ii}-Cu10-Cu8^{ii}	51.75(2)	O4-Cu5-S3^{v}	111.39(7)	Cu9-S11-Cu3	73.16(3)
S5^{ii}-Cu10-Cu2^{iii}	109.75(3)	O20-Cu5-Cu9^{iii}	91.59(9)	Cu9-S11-Cu4	132.67(4)
S7-Cu10-Cu11^{i}	118.34(3)	O20-Cu5-S9^{iii}	111.55(12)	Cu9-S11-Cu6	93.08(3)
S7-Cu10-Cu8^{ii}	103.82(3)	O20Cu5S3^{5}	113.15(13)	Cu6-S11-Cu4	89.37(3)
S7-Cu10-Cu2^{iii}	53.68(2)	O20-Cu5-O4	85.15(11)	C16-S11-Cu3	112.19(12)
S7-Cu10-S5^{ii}	143.81(3)	S1-Cu1-Cu8^{vii}	48.43(2)	C1-S1-Cu2	110.7(2)
O13-Cu10-Cu11^{i}	93.81(7)	S1Cu1O12^{6}	104.06(7)	C1-S1-Cu1	116.4(2)
O13-Cu10-Cu8^{ii}	131.04(6)	S7^{xii}-Cu1-Cu8^{vii}	95.45(3)	O19-Cu1-S7^{xii}	109.08(13)
O13-Cu10-Cu2^{iii}	110.30(6)	S7^{xii}-Cu1-S1	120.08(3)	O19-Cu1-O12^{vi}	86.18(12)
O13-Cu10-S5^{ii}	105.33(7)	S7^{xii}-Cu1-O12^{vi}	112.55(7)	Cu7-S9-Cu4^{iii}	88.32(3)
O13-Cu10-S7	110.64(7)	O12^{vi}-Cu1-Cu8^{viii}	149.39(7)	Cu7-S9-Cu9	75.55(3)
Cu4-Cu3-Cu7^{iii}	70.478(16)	O19-Cu1-Cu8^{viii}	96.46(10)	Cu7-S9-Cu5^{iii}	133.98(4)
Cu4-Cu3-Cu9	102.311(19)	O19-Cu1-S1	119.38(12)	Cu4^{iii}-S9-Cu5^{iii}	88.53(3)
Cu9-Cu3-Cu7^{iii}	122.02(2)	O2-Cu3-S3^{iv}	112.30(7)	Cu9-S9-Cu4^{iii}	136.55(4)
S11-Cu3-Cu7^{iii}	116.38(3)	Cu9-Cu7-Cu3^{iii}	119.31(2)	Cu9-S9-Cu5^{iii}	75.70(3)
S11-Cu3-Cu4	55.11(2)	Cu6-Cu7-Cu3^{iii}	98.143(19)	C13-S9-Cu7	116.26(12)
S11-Cu3-Cu9	52.99(2)	Cu6-Cu7-Cu9	74.087(17)	C13-S9-Cu4^{iii}	110.67(12)
S3^{iv}-Cu3-Cu7^{iii}	53.17(2)	S9-Cu7-Cu3^{iii}	97.25(3)	O2-Cu3-Cu4	91.12(7)
S3^{iv}-Cu3-Cu4	123.19(3)	S9-Cu7-Cu9	52.75(2)	O2-Cu3-Cu9	128.18(6)
S3^{iv}-Cu3-Cu9	101.41(3)	S9-Cu7-Cu6	125.30(3)	O2-Cu3-S11	102.24(7)
S3^{iv}-Cu3-S11	145.43(3)	O8-Cu6-Cu7	83.03(6)	O8-Cu6-S11	114.23(7)
O2-Cu3-Cu7^{iii}	109.70(6)	S1^{viii}-Cu8-Cu2^{viii}	52.38(2)	S1^{viii}-Cu8-Cu1^{viii}	47.83(2)
S3^{v}-Cu7-Cu6	54.30(2)	Cu10^{ii}-S5-Cu11^{vii}	73.66(3)	O7-Cu7-Cu3^{iii}	131.40(7)
Cu10^{ii}-S5-Cu8	77.17(3)	O7-Cu7-Cu9	108.97(7)	Cu10^{ii}-S5-Cu12^{vii}	131.72(4)
O7-Cu7-Cu6	89.38(6)	Cu8-S5-Cu11^{vii}	135.44(4)	O7-Cu7-S9	117.01(7)
Cu8-S5-Cu12^{vii}	90.94(3)	O7-Cu7-S3^{v}	101.03(7)	Cu12^{vii}-S5-Cu11^{vii}	84.23(3)
S9^{iii}-Cu4-Cu3	98.94(3)	C7-S5-Cu10^{ii}	117.52(12)	S9^{iii}-Cu4-S11	126.84(3)
C7-S5-Cu11^{vii}	105.87(11)	S11-Cu4-Cu3	53.70(2)	C7-S5-Cu8	117.35(11)
O5-Cu4-Cu3	151.49(7)	C7-S5-Cu12^{vii}	109.57(12)	O5-Cu4-S9^{iii}	109.15(7)
Cu3^{i}-S3Cu7^{v}	75.81(3)	O5-Cu4-S11	103.19(7)	O5-Cu4-O1	94.29(11)
Cu3^{i}-S3-Cu5^{v}	89.01(3)	O1-Cu4-Cu3	80.11(8)	Cu7^{v}-S3-Cu6^{v}	72.03(3)

Symmetry codes: (i) *x*, *y*−1, *z*; (ii) −*x*+1, −*y*+1, −*z*; (iii) −*x*+1, −*y*+1, −*z*+1; (iv) *x*, *y*+1, *z*; (v) −*x*+1, −*y*, −*z*+1; (vi) −*x*+1, −*y*+2, −*z*+1; (vii) −*x*+1, −*y*+2, −*z*; (viii) −*x*, −*y*+1, −*z*+1; (ix) *x*−1, *y*−1, *z*+1; (x) −*x*+2, −*y*+2, −*z*; (xi) *x*−1, *y*, *z*+1; (xii) *x*+1, *y*+1, *z*−1; (xiii) *x*+1, *y*, *z*−1.

Table S7 Hydrogen-bond geometry (Å, º) for 2

D-H···A	D-H	H···A	D···A	D-H···A
O19-H19A···O26^{xv}	0.85	2.04	2.889 (6)	179
O19-H19B···O21^{viii}	0.85	2.45	2.972 (5)	120
O20-H20A···O23	0.90	2.08	2.746 (4)	130
O20-H20B···O22^{iii}	0.90	2.26	2.947 (5)	133
O21-H21A···O24	0.87	1.91	2.727 (6)	156
O21-H21B···O23^{v}	0.82	1.91	2.717 (4)	166
O22-H22A···O27	0.85	1.82	2.666 (6)	174
O22-H22B···O26	0.85	1.90	2.664 (5)	148
O23-H23A···O3^{xiv}	0.85	1.98	2.767 (5)	154
O23-H23B···O8^{v}	0.85	2.15	2.966 (4)	161
O24-H24A···O25	0.85	1.90	2.723 (7)	161
O24-H24B···O13^{ii}	0.85	2.13	2.887 (5)	149
O25-H25A···O9	0.85	1.93	2.762 (6)	167
O26-H26A···O17	0.85	2.05	2.835 (12)	154
O26-H26A···O17A	0.85	2.24	3.01 (14)	151
O26-H26B···O14	0.85	2.09	2.707 (5)	129
O27-H27A···O28	0.85	1.86	2.688 (7)	166
O27-H27B···O2	0.85	2.17	2.914 (5)	147
O28-H28A···O9^{xvi}	0.85	2.01	2.846 (6)	168
O28-H28B···O12^{xvii}	0.85	2.22	3.009 (6)	154
C6-H6B···O3^{viii}	0.97	2.40	3.196 (6)	139

Symmetry codes: (ii) $-x+1, -y+1, -z$; (v) $-x+1, -y, -z+1$; (iii) $-x+1, -y+1, -z+1$; (v) $-x+1, -y, -z+1$; (viii) $-x, -y+1, -z+1$; (xiv) $x+1, y-1, z$; (xv) $-x, -y+2, -z+1$; (xvi) $x-1, y+1, z$; (xvii) $x-1, y, z$.

Table S8. Summarized proton conductivities of some MOFs at high humidity (>80% RH)

Materials	Proton conductivity ($S \cdot cm^{-1}$)	RH and Temperature (°C)	Ref.
Sr-SBBA	4.4×10^{-5}	98% and 25	1
$[Cd(L\text{-}tart)\text{-}(bpy)(H_2O)]_n \cdot 9n(H_2O)$	1.3×10^{-6}	95% and 85	2
$[Cd(D\text{-}tart)\text{-}(bpy)(H_2O)]_n \cdot 9n(H_2O)$	1.3×10^{-6}	95% and 85	2
$[Cd(DL\text{-}tart)\text{-}(bpy)(H_2O)]_n \cdot 6n(H_2O)$	4.5×10^{-7}	95% and 85	2
In-IA-2D-1	3.4×10^{-3}	98% and 27	3
In-IA-2D-2	4.2×10^{-4}	98% and 27	3
$\{[Gd(L)(Ox)(H_2O)]_n \cdot 3H_2O\}$	4.7×10^{-4}	95% and 80	4
Tb-DSOA	4.0×10^{-4}	98% and 53	5
β-PCMOF2	1.8×10^{-6}	85% and 50	6
PCMOF2	2.4×10^{-5}	85% and 50	6
HKUST-1	1.8×10^{-8}	70% and 90	7
NENU-3	4.76×10^{-5}	70% and 90	7
PCMOF-3	3.5×10^{-5}	98% and 25	8
Sr-SBBA	4.4×10^{-5}	98% and 25	9
$[La_2(ox)_3(H_2O)_6]\ 4H_2O$	3.35×10^{-7}	100% and 95	10
$[Zn_2(HCOO)(trz)_3]_n$	7.95×10^{-7}	98% and 50	11
1	3.63×10^{-5}	98% and 60	This work
2	2.75×10^{-5}	98% and 60	This work

References

1. Kundu, T.; Sahoo, S. C.; Banerjee, R. *Chem. Commun.* **2012**, *48*, 4998-5000.

2. Parshamoni, S.; Jena, H. S.; Sanda, S.; Konar, S. *Inorganic Chemistry Frontiers*, **2014**, *1*, 611-620.

3. Panda, T.; Kundu, T.; Banerjee, R. *Chem. Commun.* **2012**, *48*, 5464-5466.

4. Biswas, S.; Chakraborty, J.; Singh Parmar, V.; Bera, S. P.; Ganguli, N.; Konar, S. *Inorganic chemistry* **2017**, *56*, 4956-4965.

5. Dong, X. Y.; Wang, R.; Wang, J. Z.; Zang, S. Q.; Mak, T. C. *Journal of Materials Chemistry A*, **2015**, *3*, 641-647.

6. S. Kim, K. W.; Dawson, B. S.; Gelfand, Taylor, J. M.; Shimizu, G. K. *Journal of the American Chemical Society* **2013**, *135*, 963-966.

7. Liu, Y.; Yang, X.; Miao, J.; Tang, Q.; Liu, S.; Shi, Z.; Liu, S. *Chem. Commun.* **2014**, *50*, 10023-10026.

8. Shigematsu, A.; Yamada, T.; Kitagawa, H. *Journal of the American Chemical Society* **2011**, *133*, 2034-2036.

9. Taylor, J. M.; Mah, R. K.; Moudrakovski, I. L.; Ratcliffe, C. I.; Vaidhyanathan, R.; Shimizu, G. K. *Journal of the american chemical society* **2010**, *132*, 14055-14057.

10. Kundu, T.; Sahoo, S. C.; Banerjee, R. *Chem. Commun.* **2012**, *48*, 4998-5000.

11. Ishikawa, R.; Ueno, S.; Yagishita, S.; Kumagai, H.; Breedlove, B. K.; Kawata, S. *Dalton Trans* **2016**, *45*, 15399-15405.

12. Lu, J. N.; Zhou, S. F.; Zhang, S. J.; Zhang, C. X.; Wang, Q. L. *European Journal of Inorganic Chemistry* **2019**, *2019*, 794-799.

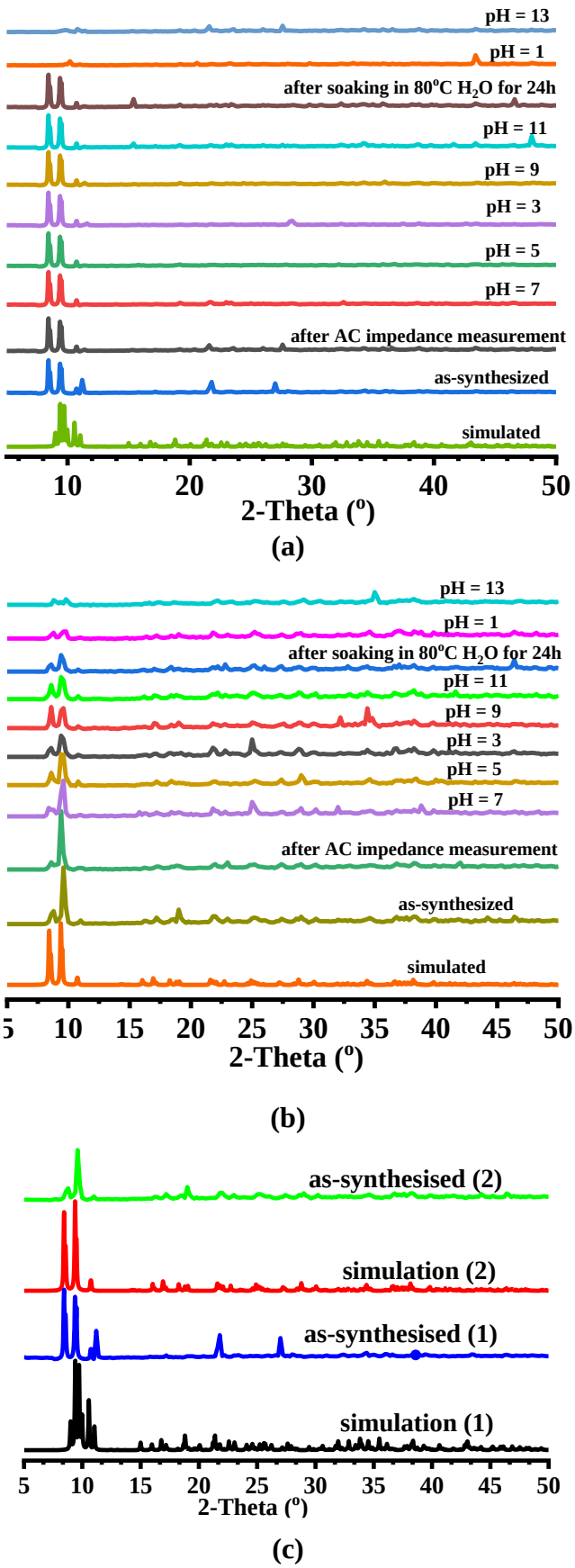

Fig. S1 PXRD patterns of **1** (a), **2** (b), and (c) PXRD patterns of **1** and **2**: The simulated ones from the single-crystal data, and as-synthesized.

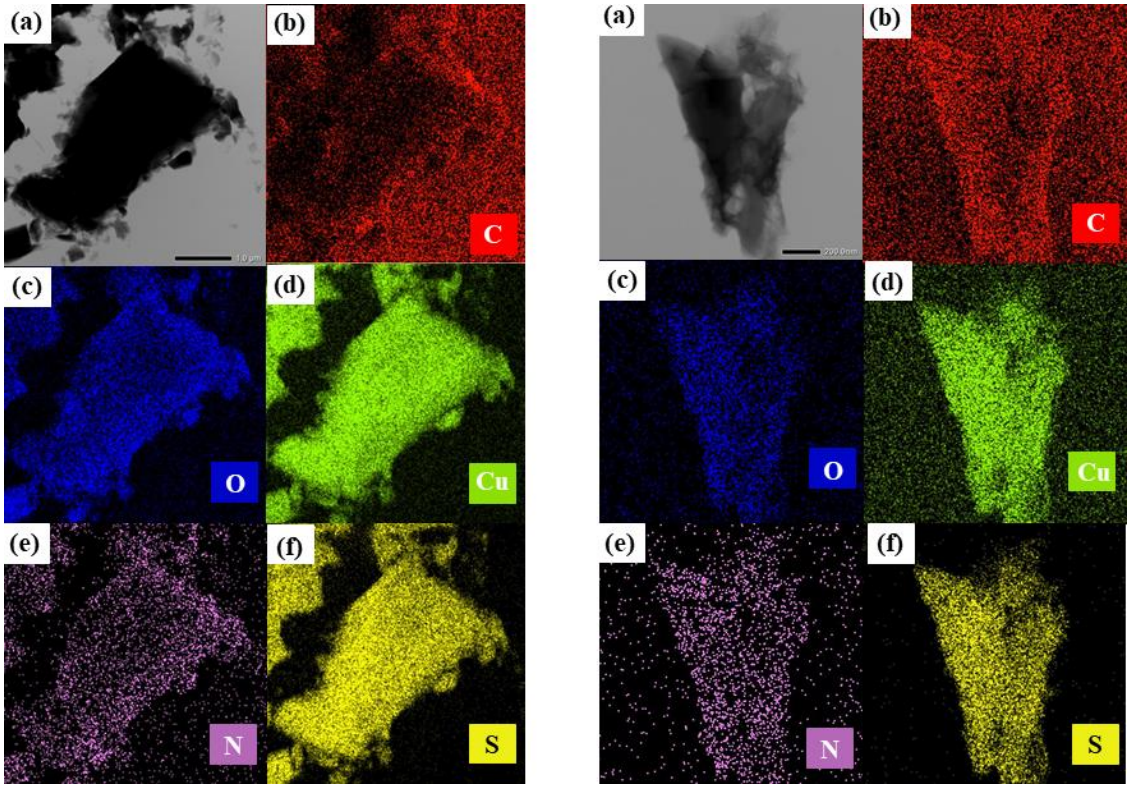

Figure. S2 (a-f) TEM and elemental mapping images of MOFs **1** (left) and **2** (right).

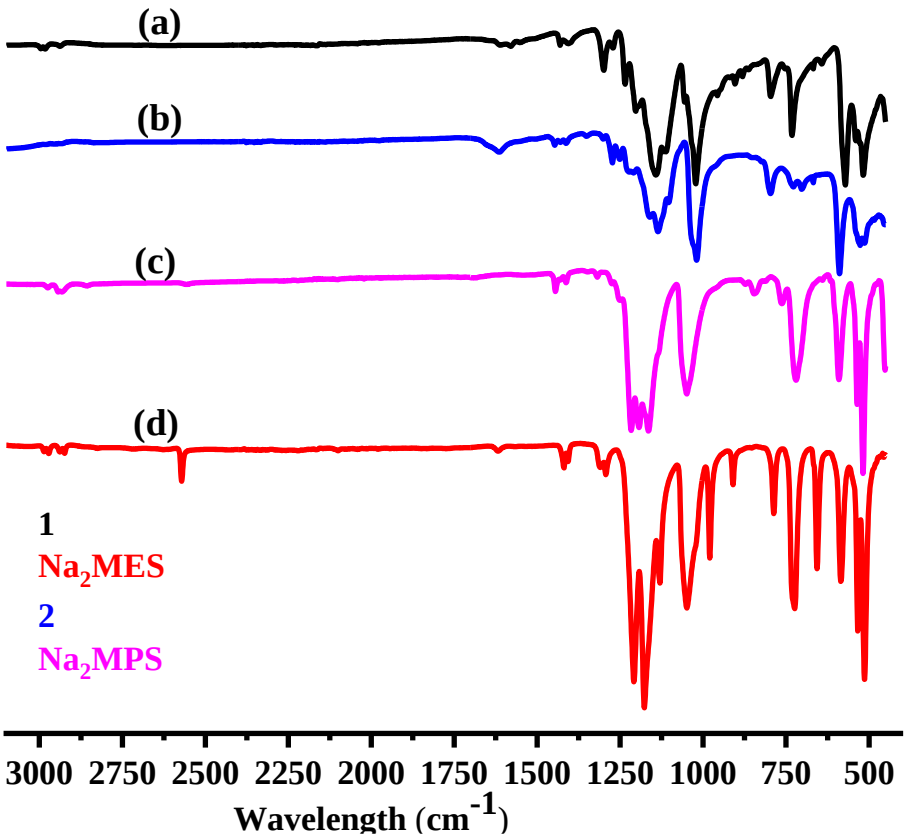

Fig. S3 The IR spectra of **1** (a), **2** (b), Na_2MPS (c), and Na_2MES (d).

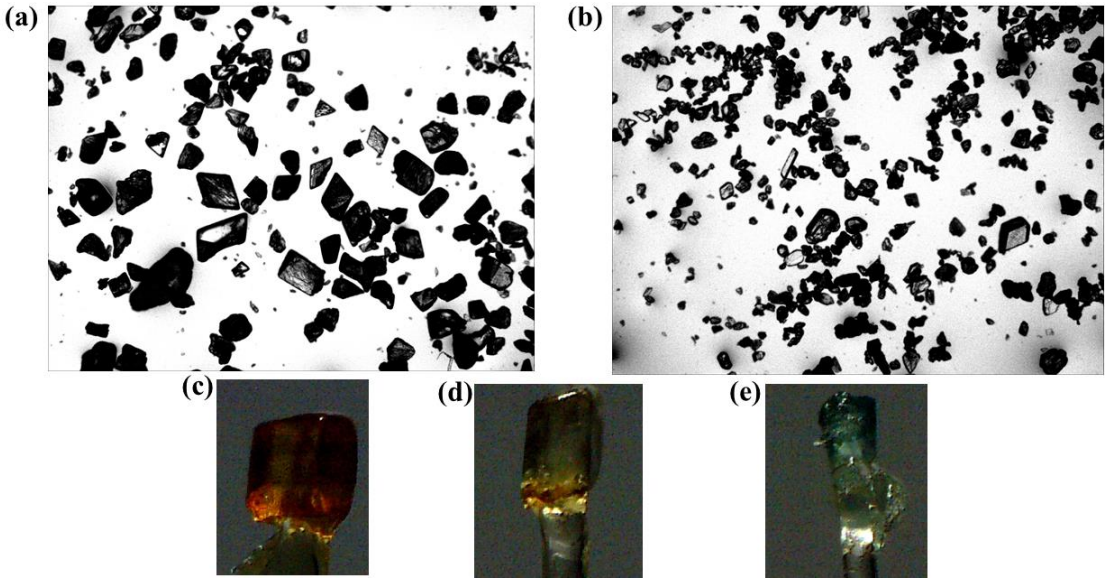

Fig. S4 Sample crystal photographs of **1** (a) and **2** (b). Single-crystal photographs of **1** (c), **2** (d), and diaqua-bis(pyridine-4-carboxylate-N)-copper(II) monohydrate (e).

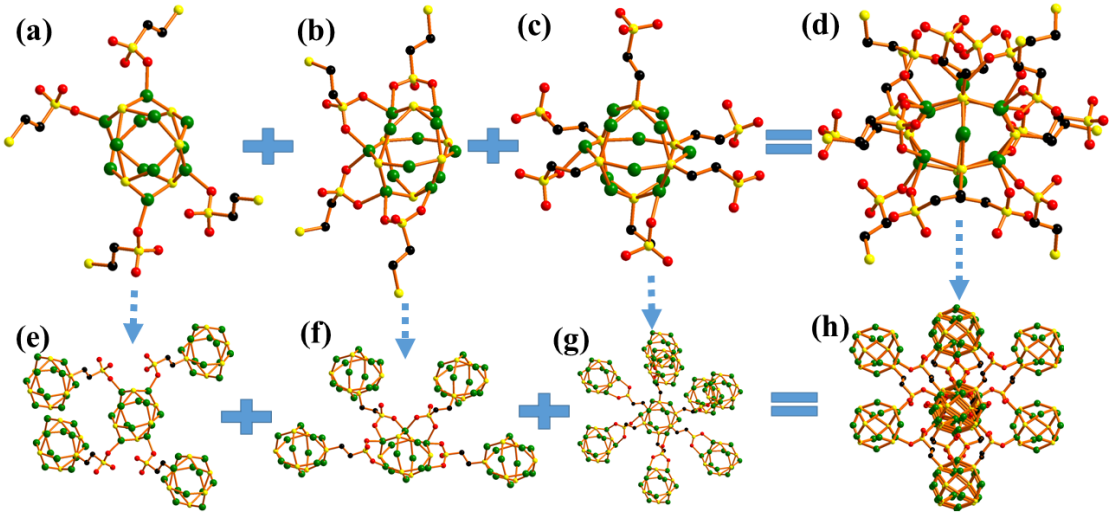

Fig. S5 The schematic view of the $Cu_{12}S_6$ cluster and fourteen MES^{2-} in **1**.

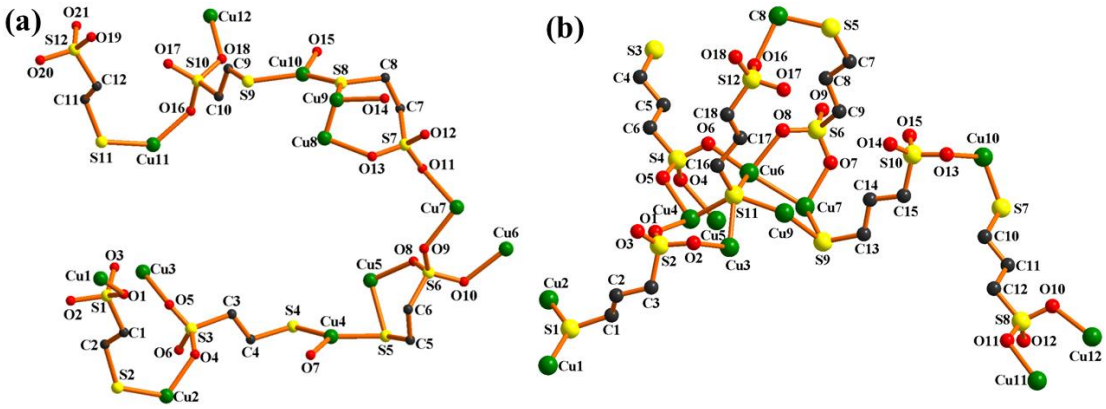

Fig. S6 The asymmetric unit of (a) for **1** and (b) for **2**. All H-atoms have been omitted for clarity, and all coordinated and free H_2O also have been removed in 2.

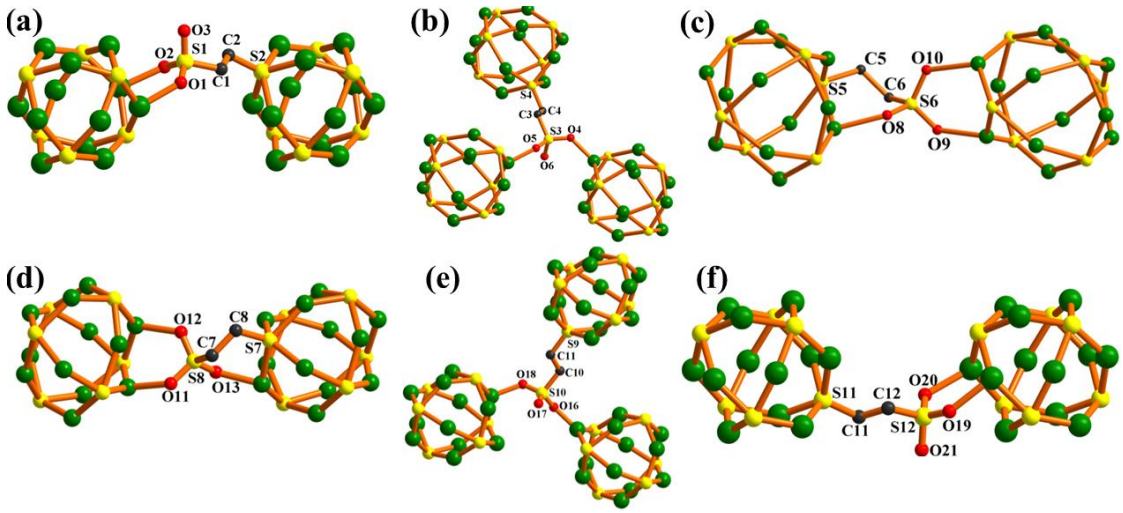

Fig. S7 (a-f) The mode of $Cu_{12}S_6$ cluster connected by MES^{2-} ligand in **1**.

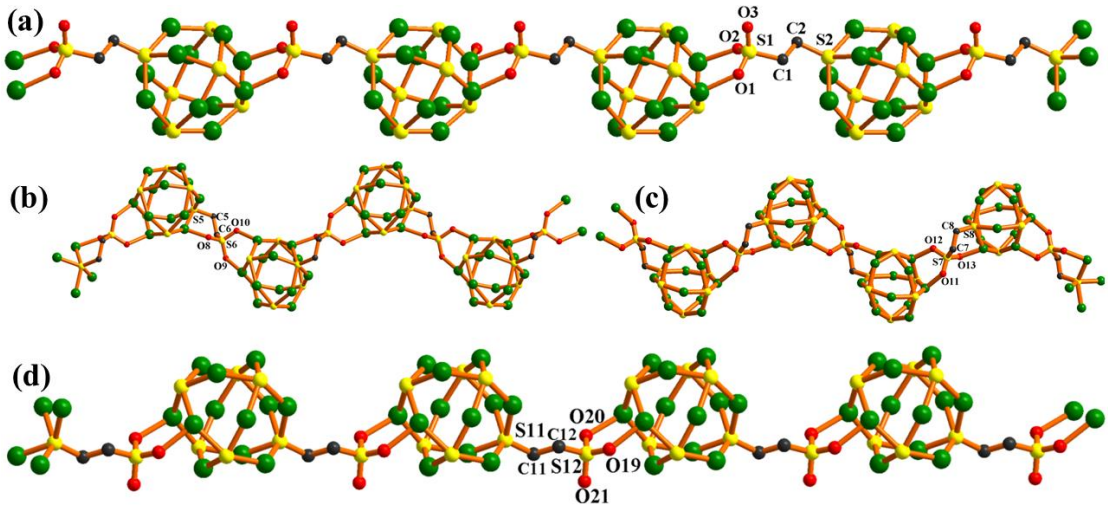

Fig. S8 (a-d) The 1D $[(Cu_{12}S_6)(MES)]_n$ chain in **1**, involved in S-containing ligands abbreviated as $S_{1\text{-}2}$, $S_{5\text{-}6}$, $S_{7\text{-}8}$ and $S_{11\text{-}12}$, respectively.

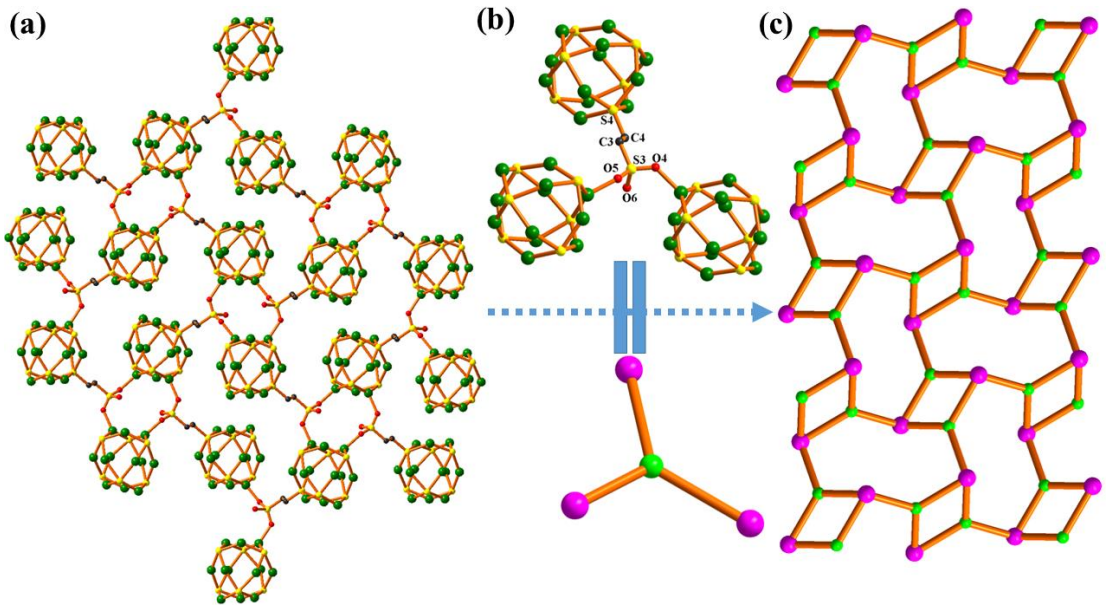

Fig. S9 (a) The 2D $[(Cu_{12}S_6)(MES)]_n$ network in **1**, involved in S-containing ligands abbreviated as $S_{3\text{-}4}$; (b) The MES^{2-} linked three $Cu_{12}S_6$ clusters was simplified as a 3-connected node; (c) The 2D $[(Cu_{12}S_6)(MES)]_n$ network was simplified as a uninodal 3-c Shubnikov plane topology with a point (Schlafli) symbol for net: $\{4\cdot8^2\}$.

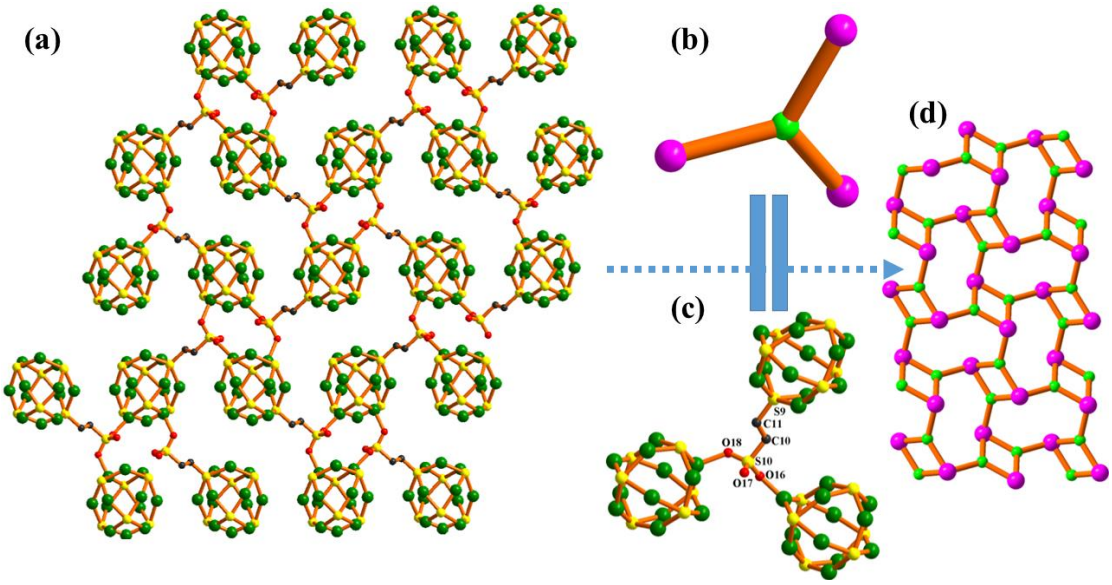

Fig. S10 (a) The 2D $[(Cu_{12}S_6)(MES)]_n$ network in **1**, involved in S-containing ligands abbreviated as $S_{9\text{-}10}$; (b-c) The MES^{2-} linked three $Cu_{12}S_6$ clusters was simplified as a 3-connected node; (d) The 2D $[(Cu_{12}S_6)(MES)]_n$ network was simplified as a uninodal 3-c Shubnikov plane topology with a point (Schlafli) symbol for net: $\{4\cdot8^2\}$.

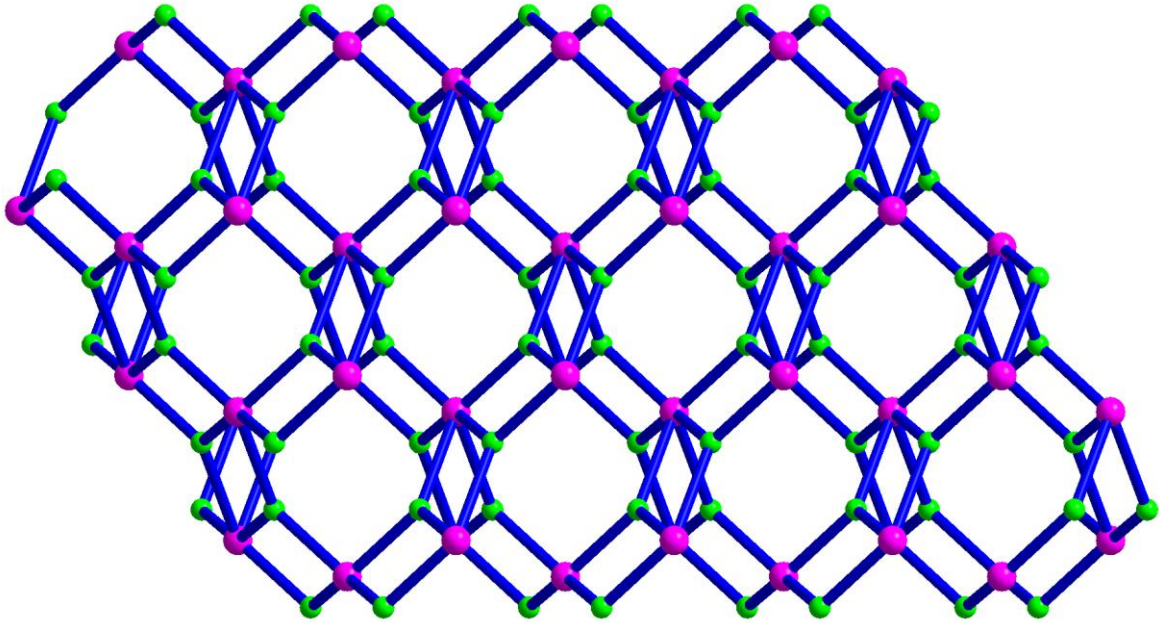

Fig. S11 The two 2D topologies assemble a 2-nodal 3,6-c ant/anatase net with a point symbol of $\{4^2\cdot6\}_2\{4^4\cdot6^2\cdot8^8\cdot10\}$, involved in S-containing ligands abbreviated as $S_{3\text{-}4}$ and $S_{9\text{-}10}$.

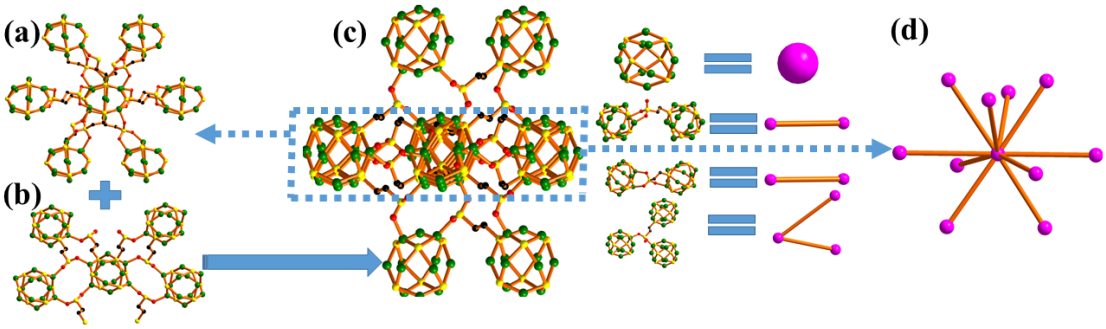

Fig. S12 (a-d) The diagram of the $Cu_{12}S_6$ clusters was simplified as a 10-connected node in **1**.

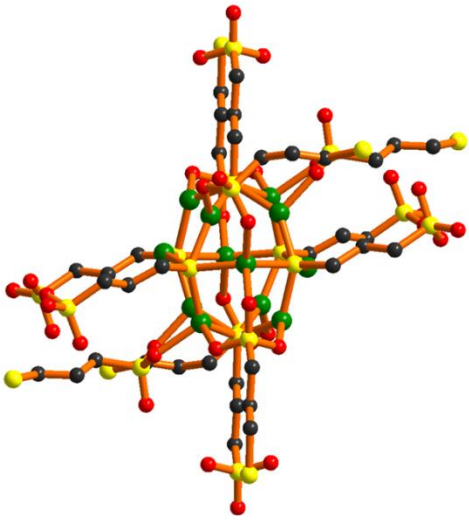

Fig. S13 The scheme of a $Cu_{12}S_6$ cluster connected with twelve MES^{2-} ligands in **2**.

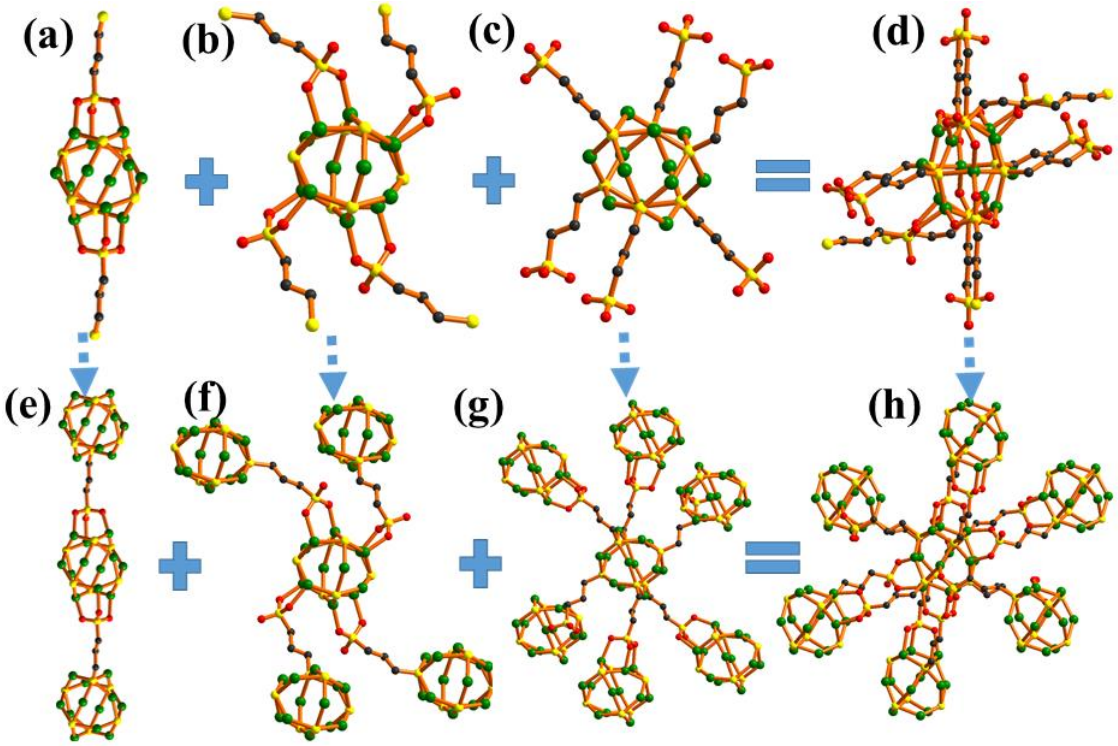

Fig. S14 (a-h) The schematic view of the $Cu_{12}S_6$ cluster and twelve MES^{2-} in **2**.

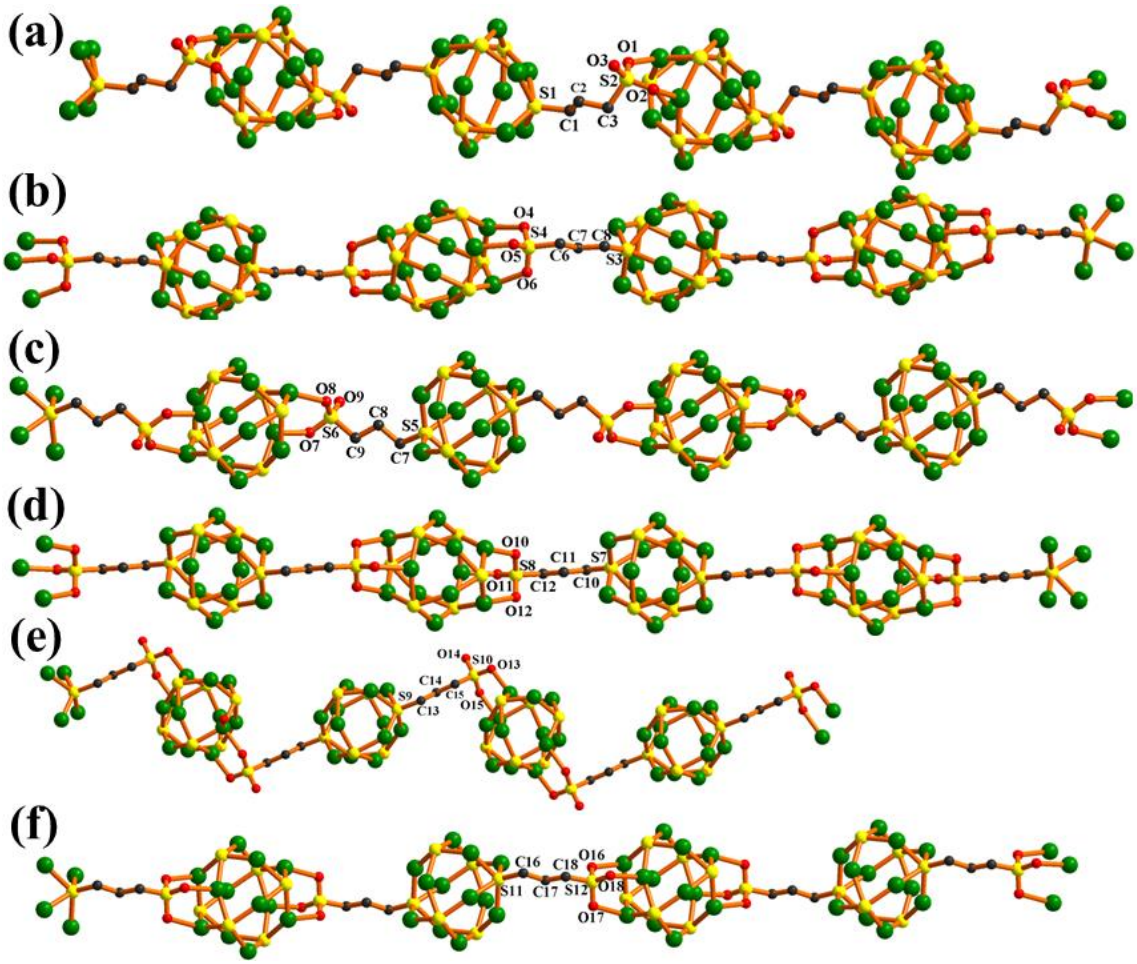

Fig. S15 (a-f) The 1D $[(Cu_{12}S_6)(MPS)]_n$ chain in **2**, involved in S-containing ligands abbreviated as $S_{1\text{-}2}$, $S_{3\text{-}4}$, $S_{5\text{-}6}$, $S_{7\text{-}8}$, $S_{9\text{-}10}$ and $S_{11\text{-}12}$, respectively.

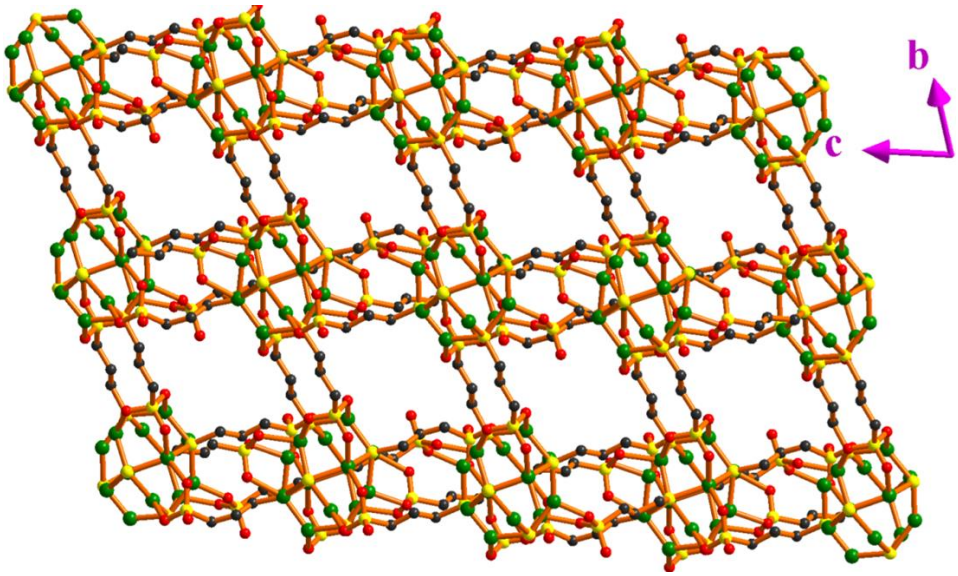

Fig. S16 View of the 3D $Cu_{12}S_6$ cluster based organic framework of **2** from *a* direction.

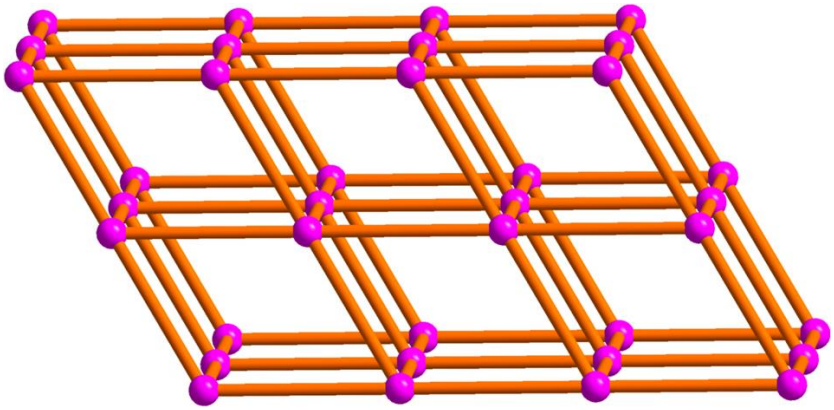

Fig. S17 View of a 6-connected **pcu** primitive cubic network with a Schläfli symbol $\{4^{12}.6^3\}$ of **2**.

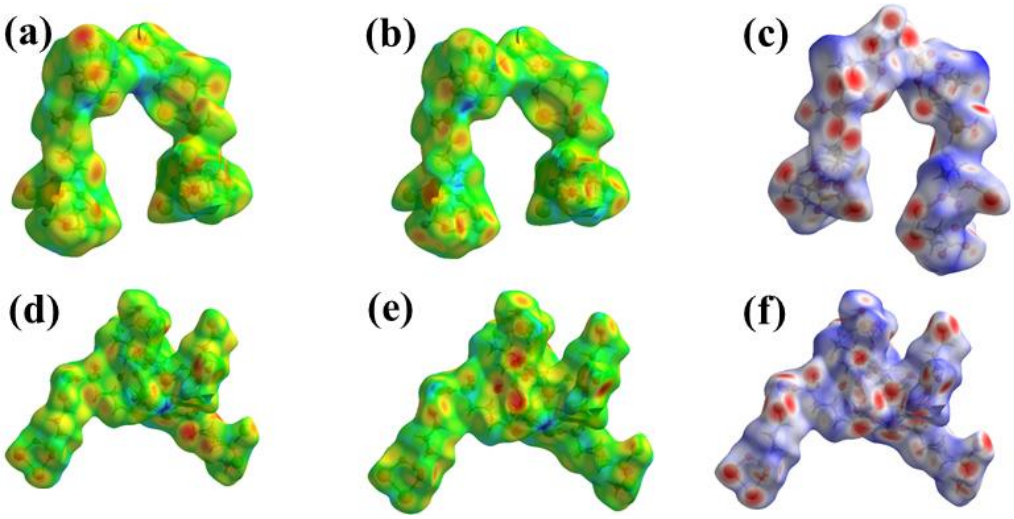

Fig. S18 Hirshfeld surface of **1** with d_i (a), d_e (b) and d_{norm} (c) mapped in colour; the Hirshfeld surface of **2** with d_i (d), d_e (e) and d_{norm} (f) mapped in colour; in all cases, red represents the closest contacts, and blue represents the most distant contacts.

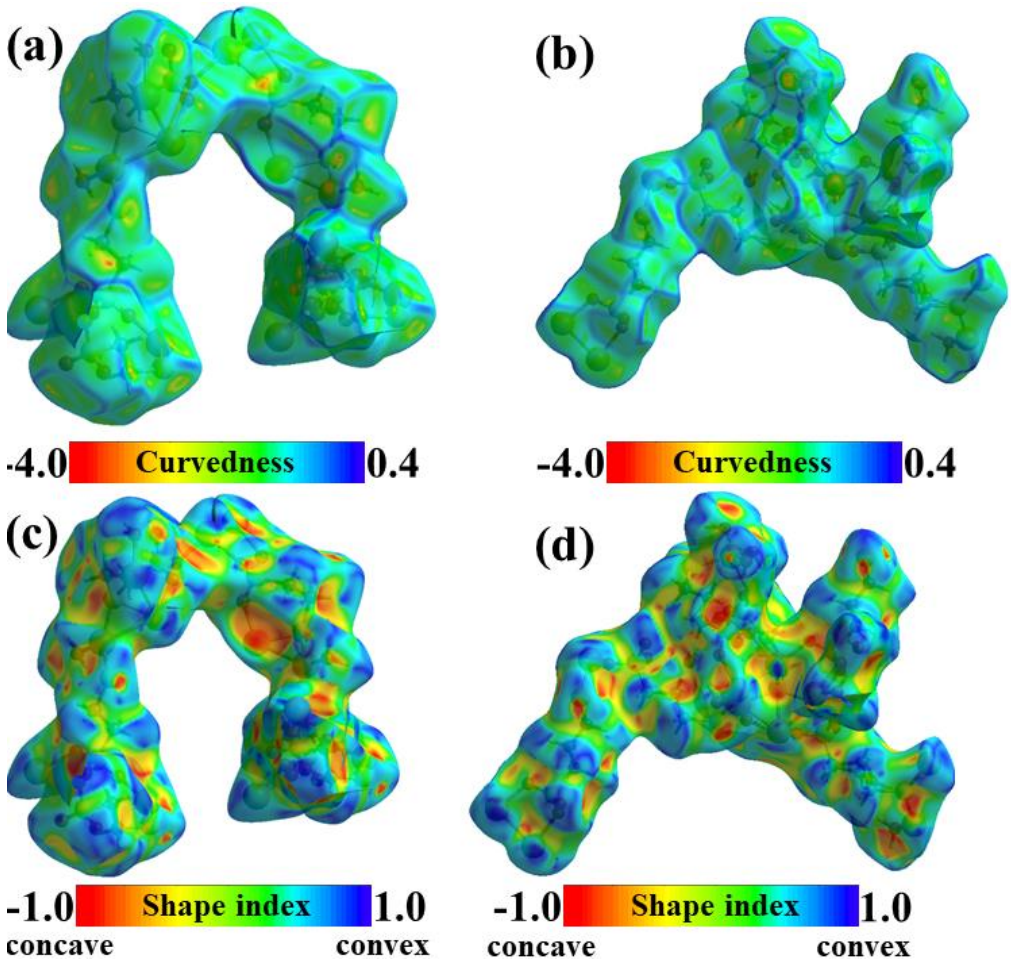

Fig. S19 (a, c) Hirshfeld surface of **1** with curvedness and shape index mapping; (b, d) the Hirshfeld surface of **2** with curvedness and shape index mapping.

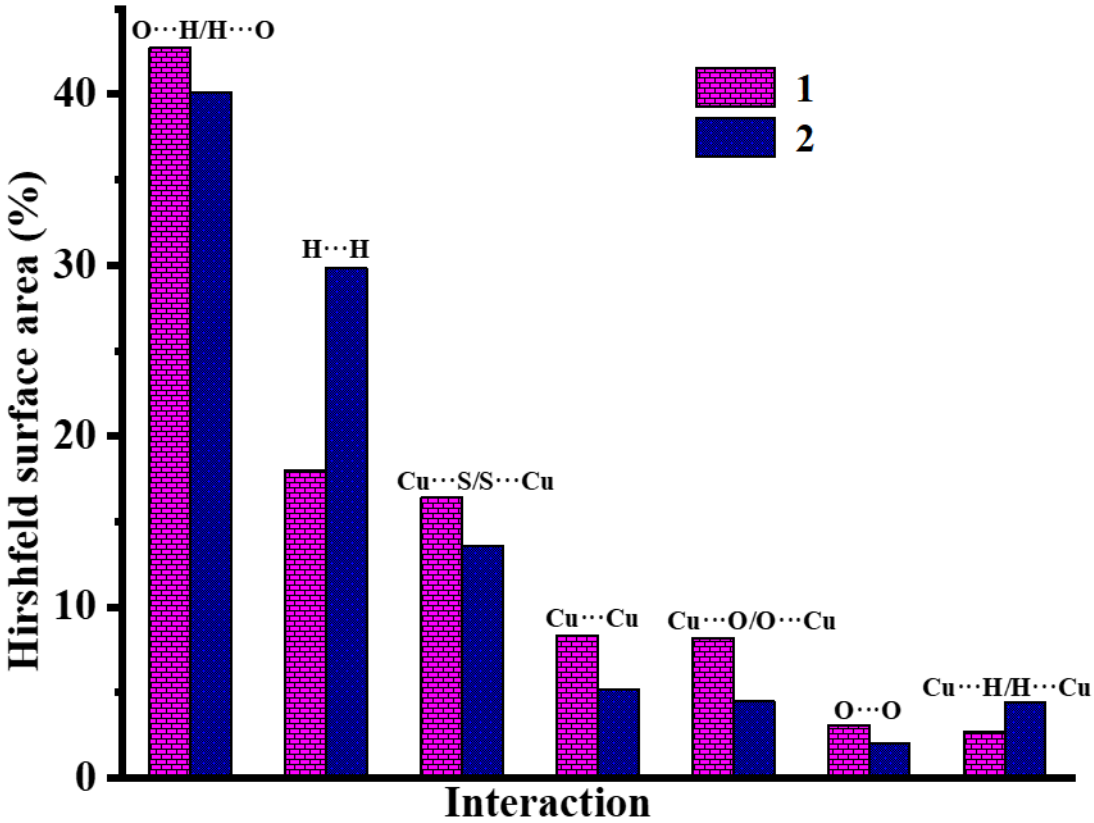

Fig. S20 Relative contributions to Hirshfeld surface area for various intermolecular contacts in **1** and **2**.

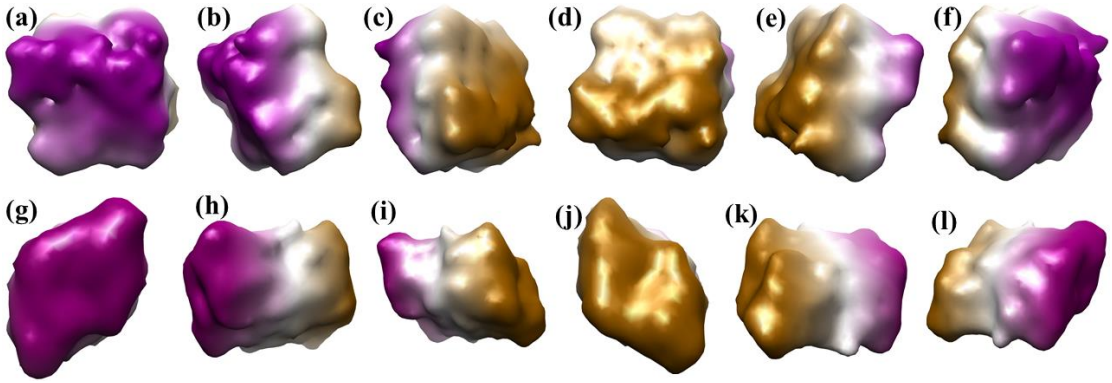

Fig. S21 The surface of **1** (a-f) and **2** (g-l) calculated via 3V Volume Assessor program by rolling a virtual probe (0.8 Å) on the surface viewed along six different orientations.

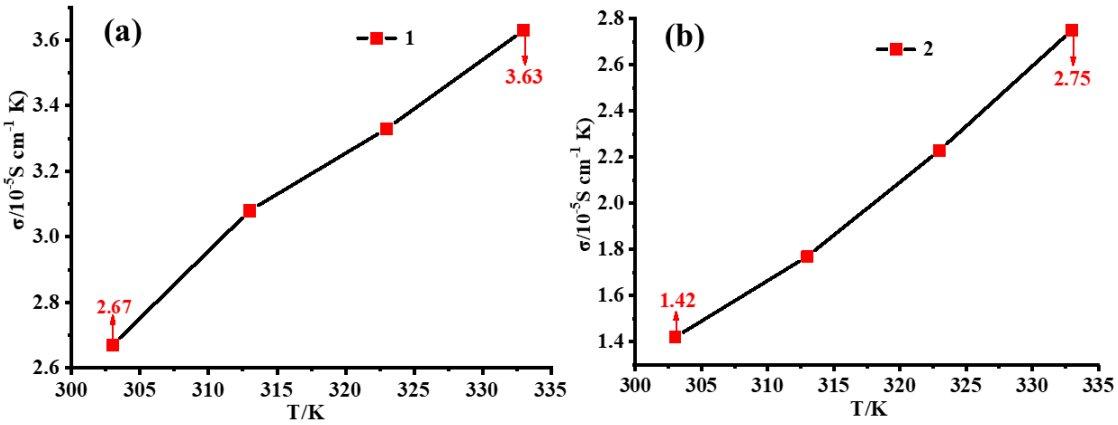

Fig. S22 The conductivity **1**/Nafion (a) and **2**/Nafion (b) at different temperature.

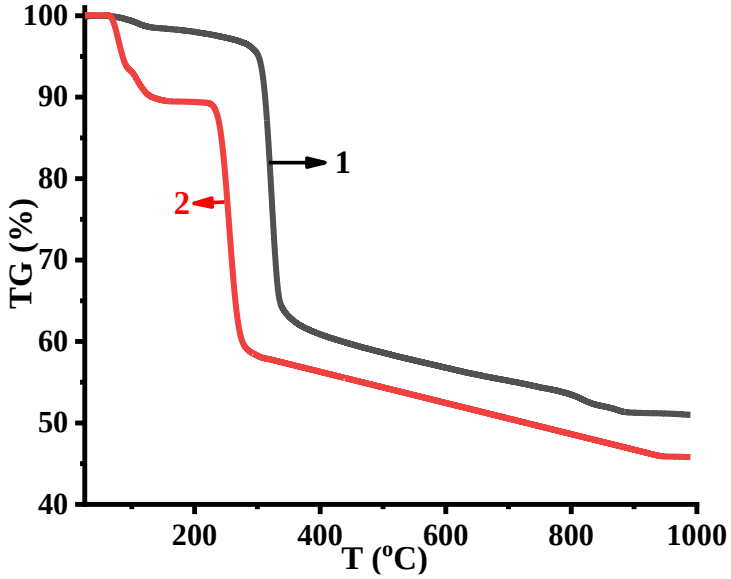

Fig. S23 The TG curves for **1** and **2**.